ISSN 1995-0802, Lobachevskii Journal of Mathematics, 2020, Vol. 41, No. 8, pp. 1545–1553. © Pleiades Publishing, Ltd., 2020.

Optimizing the Multimode Brownian Oscillator Model for the Optical Response of Carotenoids in Solution by Fine Tuning of Differential Evolution

R. Y. Pishchalnikov[1*], A. A. Bondarenko[2], and A. A. Ashikhmin[3***]**

(Submitted by E. E. Tyrtyshnikov)

[1] *Prokhorov General Physics Institute of the Russian Academy of Sciences, Moscow, 119991 Russia*

[2] *Keldysh Institute of Applied Mathematics of the Russian Academy of Sciences, Moscow, 125047 Russia*

[3] *Pushchino Scientific Center for Biological Research of Russian Academy of Sciences, Institute of Basic Biological Problems, Russian Academy of Sciences, Pushchino, 142290 Russia*

Received April 4, 2020; revised April 20, 2020; accepted April 21, 2020

Abstract—During last twenty years, the Differential evolution algorithm (DE) has proved to be one of the powerful methods to solve minimization problems for multidimensional functions. Being a member of the family of evolutionary optimization algorithms, its main principle is based upon the concepts of natural selection and mutation. In this study, we test the potential of DE to find a proper set of parameters for the multimode Brownian oscillator model, which was then used to simulate absorption lineshapes of carotenoid molecules in solution: spheroidene and spheroidenone. This theory assumes that the correlation function of a particular electronic state of the carotenoid is calculated using the semiclassical spectral density function. Considering our previous studies on photosynthetic pigments, we employed several DE strategies to do fitting of the carotenoid experimental spectra. We found that simulated absorption spectra are very sensitive to several parameters that characterize carotenoid vibronic modes, namely, Huang–Rhys factors. Fine tuning of DE crossover parameter (Cr) and the scaling factor (F) provided acceptable convergence of the algorithm. It appears that to get good convergence of DE, a certain spectral range of carotenoid absorption from 400 to 600 nm must be chosen. This fact can be explained by the limitations of the applied theory, which simply does not predict properly the carotenoid absorption at higher frequencies.

DOI: 10.1134/S1995080220080156

Keywords and phrases: *differential evolution, parallel programming, carotenoids, absorption spectrum, cumulant expansion, multimode Brownian oscillator model.*

1. INTRODUCTION

Carotenoids are pigments that are widespread in nature [1]. They are contained in pigment-protein complexes of photosynthetic species such as plants, cyanobacteria and algae [2]. Knowing their optical properties is of extreme importance, since carotenoids participate in the primary processes of energy migration in photosynthesis and are responsible for the protection of the photosynthetic mechanism from excess incident light [3, 4].

The absorption bands of carotenoids usually peak at 400–600 nm in the visible region. That is why carotenoids are orange, red, and yellow. The basis of the chemical structure of carotenoids is a polyene hydrocarbon chain. Depending on what kind of residue terminates the polyene chain and the number of conjugated double bonds in the chain, the optical properties of carotenoids can vary significantly [5]. In

*E-mail: rpishchal@kapella.gpi.ru

**E-mail: bondaleksey@gmail.com

***E-mail: ashikhminaa@gmail.com

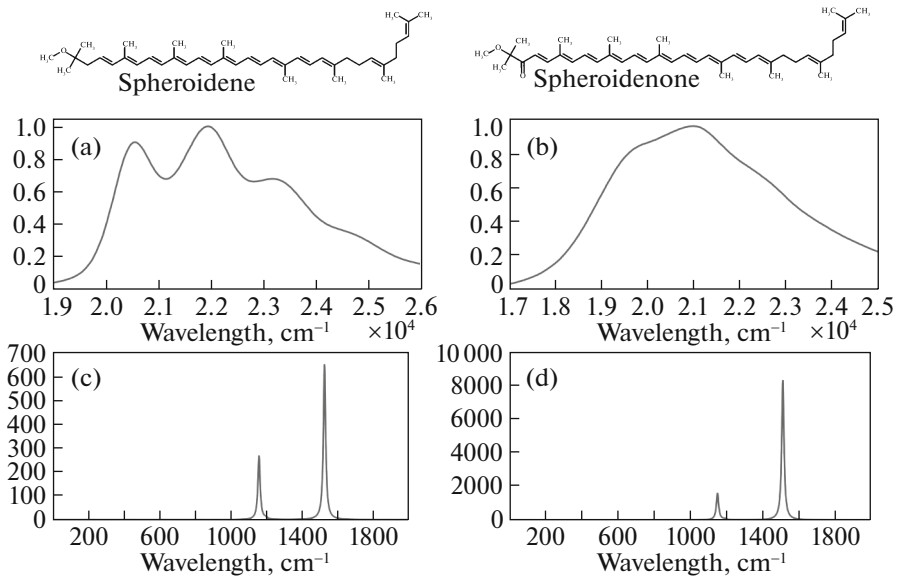

Fig. 1. Chemical structure of spheroidene (left) and spheroidenone (right) and their experimentally measured absorption spectra (a, b) in methanol/acetone solution at room temperature, respectively. The calculated spectral densities $C''(\omega)$ for spheroidene and spheroidenone according to Eq. (7) are shown in (c, d). Parameters of the $C''(\omega)$ modeling were taken from [9].

this study, we simulate the absorption spectra of spheroidene and spheroidenone. These carotenoids are obtained from strains of the anaerobic purple bacterium *Rhodobacter sphaeroides* [6]. Their chemical structures and absorption spectra are shown in Fig. 1. The quantitative relationship between the carotenoid structure and its optical properties can be specified by applying the multimode Brownian oscillator model [7]. This theory allows for simulation the optical response of a system consisting of electronic states interacting with vibronic modes and the local surrounding. The electronic states of carotenoids have rather unusual properties: the lowest state $|S_1\rangle$ is optically forbidden and cannot be populated by direct excitation [8]. The carotenoid absorption spectrum at 400–600 nm belongs to the allowed $|S_2\rangle$ state. Also, there are so-called $|S^*\rangle$ electronic states, but the discussion of their optical properties lies outside the scope of this study. The simulation of $|S_2\rangle$ absorption profile is our immediate goal.

The spectral density of nuclear vibrations is the key quantity in modeling the absorption spectra of dye molecules in a solvent. It is a very temperature-independent function. To evaluate it, a set of parameters must be specified that is needed to describe a vibrational mode, including the intensity of the electron-phonon coupling [7, 9–11]. Using the spectral density, we can calculate correlation functions of an electronic transition moment and then the corresponding absorption spectrum. If the frequency of a vibronic mode can be determined directly from an experiment, the electron-phonon coupling is estimated by a dimensionless parameter called the Huang–Rhys factor [7]. To calculate the absorption spectrum properly, the required number of vibronic modes can vary up to several dozens for different types of dye molecules [11]. Taking into account that in addition to the vibronic mode parameters to be found and those of the electronic state, carotenoid absorption spectra simulation can be considered as a case of an optimization problem and a real challenge for any multidimensional optimizer, particularly for DE.

The optimization problem is the process of finding a set of variables that produces the best values of an objective function in which the feasible domain of variables is restricted by constraints [12]. For instance, in the dye molecule optical response simulation, the objective function might be the χ^2 function calculated considering a measured spectrum as the target function and a simulated spectrum as the trial function [11]. There are classes of optimization problems in which a solution cannot be found without a brute force search. If these tasks have large dimensionality, the implementation of the brute force search is practically impossible because of the extremely large time costs. In these cases, the methods based on evolutionary principles are used to solve such kind of problems.

Evolutionary algorithms belong to a variety of population methods that involve adaptation of successful generations of candidate solutions. The main feature of these algorithms is that having a large number

of free variables, they can avoid getting stuck in a local minimum. The family of evolutionary algorithms consists of genetic algorithms [13], evolutionary programming [14], particle swarm optimization [15], and differential evolution [16, 17]. To fit the carotenoid absorption, we use DE optimized for the needs of our simulations [11]. Unlike traditional evolutionary algorithms, DE creates a new generation of parameters perturbing the current generation with scaled difference of randomly selected population members. Detailed introduction to DE can be founding comprehensive surveys of the topic [18, 19].

Analysis and interpretation of spectral properties of carotenoids has already been done in many studies [20–24]; however, considering our experience in modeling the absorption spectra of carotenoids in different environments [9, 25], it should be noted that not all parameters of the multimode Brownian oscillator model can be determined unambiguously. Compared to other dye molecules, carotenoids have only four distinct vibronic modes [1] at 600–2000 cm^{-1} that makes them a proper system to test the power of DE.

2. THEORY

The absorption spectra at 400–600 nm of the carotenoids under consideration can be modeled by a two-level system of a ground $|g\rangle$ state and an exited $|e\rangle$ electronic state. The electronic excited state of the carotenoids in this spectral region corresponds to the so-called optically allowed $|S_2\rangle$ state. The total Hamiltonian of the system, including the sets of vibronic modes, is written in the form

$$H_{tot} = |g\rangle H_g(\mathbf{q})\langle g| + |e\rangle H_e(\mathbf{q})\langle e|, \tag{1}$$

$$H_g(\mathbf{q}) = \sum_j^N \left(\frac{p_j^2}{2m_j} + \frac{1}{2}m_j\omega_j^2 q_j^2\right), \tag{2}$$

$$H_e(\mathbf{q}) = h\omega_{eg}^0 + \sum_j^N \left(\frac{p_j^2}{2m_j} + \frac{1}{2}m_j\omega_j^2 (q_j + d_j)^2\right), \tag{3}$$

$H_g(\mathbf{q})$ and $H_e(\mathbf{q})$ are the ground and the exited state Hamiltonians; ω_{eg}^0 is the energy gap between $|g\rangle$ and $|e\rangle$; p_j, m_j, ω_j, and q_j are the effective moments, masses, frequencies, and coordinates of vibronic modes; d_j is the displacement parameter corresponding the deformation of the $|e\rangle$ potential curve. N is the number of modes.

The multimode Brownian oscillator model assumes that each vibronic mode of the system described by H_{tot} is coupled to the set of bath modes. Such assumption allows taking into account contributions of the low and high frequencies of nuclear vibrations in one expression for the spectral density. In this case H_{tot} is modified by adding H_{VB} part:

$$H_{tot} = H_g + H_e + H_{VB}, \tag{4}$$

$$H_{VB} = \sum_n^M \left[\frac{p_n^2}{2m_n} + \frac{1}{2}m_n\omega_n^2\chi_n^2 - \chi_n\sum_j c_{nj}q_j + \frac{\sum_j c_{nj}^2 q_j^2}{2m_n\omega_n^2}\right], \tag{5}$$

where M is the number of bath modes; p_n, m_n, and ω_n, are parameters of the n bath mode; c_{nj} are the effective couplings of the jth vibronic mode and the nth bath mode. The dynamics of electronic states is described by the density operator $\rho(t)$. The thermal equilibrium conditions of the ground state determine the initial states of the system: $\rho(-\infty) = |g\rangle\rho_g\langle g|$, where $\rho_g = \exp(-\beta H_g)/\mathrm{Tr}\ \exp(-\beta H_g)$ and $1/\beta = kT$, T is the temperature.

When the system under consideration interacts with an external electric field, the optical response is defined by the polarization of the matter $P(\mathbf{r},t)$. The linear polarization $P(\mathbf{r},t)^{(1)}$ ($P(\mathbf{r},t)$ decomposition to the 1st order of the field) controls the absorption of the system [7]

$$P(\mathbf{r},t)^{(1)} = -\frac{i}{h}\int_0^\infty dt_1 E(\mathbf{r},t-t_1)S^{(1)}(t_1), \tag{6}$$

$E(\mathbf{r}, t-t_1)$ is the electric field; $S^{(1)}(t_1)$ is the linear response function, which carries the system information, and its dynamics is determined by the density operator $\rho(t)$. For a multilevel system, for example, one that is described by equations (1)–(5), $S^{(1)}(t_1)$ is calculated applying the cumulant expansion technique [26, 27]. Considering this technique, the spectral density $C''(\omega)$ and the corresponding correlation functions $C(t)$ of $|g\rangle \to |e\rangle$ transition for the multimode Brownian oscillator model can be estimated by using the path integral approach [28]:

$$C''(\omega) = \sum_j \frac{2S_j\omega_j^3\omega\gamma_j}{(\omega_j^2-\omega^2)+\omega^2\gamma_j^2}. \tag{7}$$

This expression already contains a set of effective parameters $\{\omega_j, S_j, \gamma_j\}$ that are used in modeling of carotenoid absorption instead of the microparameters in equations (2), (3), and (5), where S_j is the Huang–Rhys factor that is proportional to the electron-phonon coupling energy between an electronic state and the jth vibronic mode and γ_j is the damping factor of the jth vibronic mode. When the spectral density is evaluated, the $g(t)$ lineshape function can be obtained as follows:

$$g(t) = \frac{1}{2\pi}\int\limits_{-\infty}^{\infty} d\omega \frac{1-\cos\omega t}{\omega^2}\coth(\beta\hbar\omega/2)C''(\omega) - \frac{i}{2\pi}\int\limits_{-\infty}^{\infty} d\omega \frac{\sin(\omega t)-\omega t}{\omega^2}C''(\omega), \tag{8}$$

where $g(t)$ encapsulates the temperature dependence and the contributions of each vibronic mode to absorption spectrum introducing so-called homogeneous broadening of a state. Taking into account the inhomogeneous broadening, the resulting expression for the absorption lineshape is given as

$$\sigma_{abs}(\omega) = \frac{1}{\pi}Re\int\limits_0^{\infty} dt\, e^{i(\omega-\Omega_{eg})t}e^{-g(t)}e^{-\frac{1}{2}(\Delta t)^2}, \tag{9}$$

where Ω_{eg} is the frequency of $|g\rangle \to |e\rangle$ electronic transition, $\Delta = FWHM/2\sqrt{2\ln 2}$ is the standard deviation of the Gaussian distribution that emulates the inhomogeneous broadening, and $FWHM$ is the full width at the half maximum.

3. DIFFERENTIAL EVOLUTION

Numerical integration of equation (9) gives the simulated carotenoid absorption spectrum $\sigma_{abs}(\omega_k)$, where ω_k is a set of frequencies that matches the frequencies at which the experimental absorption spectrum $I(\omega_k)$ was measured. In fact, the arguments of $\sigma_{abs}(\omega_k)$ should be written as follows $\sigma_{abs}(\omega_k, x_i^{(g)})$. Here, $x_i^{(g)} = \{\Omega_{eg}, FWHM, \omega_j, S_j, \gamma_j\}$ are the input parameters of the fitting absorption procedure that employs DE to optimize the objective function

$$f(x_i^g) = \chi^2 = \frac{1}{K}\sum_{k=1}^{K}\frac{(I(\omega_k)-\sigma_{abs}(\omega_k, x_i^{(g)}))^2}{\sigma_{abs}(\omega_k, x_i^{(g)})}, \tag{10}$$

where K is length of ω_k array, and the g index numerates the current generation of DE.

DE searches for a global optimum point in a d-dimensional space of real variables $\Omega \subseteq \mathbb{R}^d$. Each vector $x_i^{(g)} = \{x_{i,1}^{(g)}, x_{i,2}^{(g)}, \ldots, x_{i,d}^{(g)},\}$ forms a candidate solution to the multi-dimensional optimization problem, where $g = 0, 1, \ldots, Gen_{max}$ and $i = 1, 2, \ldots, Np$. The search begins with a randomly initiated population of d-dimensional real vectors in a certain range, since the values of the parameters are related to the physical components that have natural bounds $x_{min,l} = \{x_{min,1}, x_{min,2}, \ldots, x_{min,d}\}$ and $x_{max,l} = \{x_{max,1}, x_{max,2}, \ldots, x_{max,d}\}$. To initialize the jth component of the ith decision vector, we use $\mathrm{rand}_{\mathrm{i,j()}}$, which returns uniformly distributed random number lying between 0 and 1.

After initialization, DE creates a mutation vector $v_i^{(g)}$ corresponding to each population member (target) vector $x_i^{(g)}$. In Fig. 2 we describe one of the frequently used mutation strategies; for other strategies see [19]. The indices $r1$, $r2$ and $r3$ are mutually exclusive integers randomly chosen from the

```
#step 1 initialization
1 for i=1,…,Np
2   for j=1,…,d
3     x(0)i,j=xmin,j + randi,j()(xmax,j − xmin,j)

#main calculations
4 for g=1,…,Genmax
#step 2 mutation
5   for i=1,…,Np
6     for j=1,…,d
7       v(g)i = x(g)r3 + F*(x(g)r1−x(g)r2)
#step 3 crossover
8   for i=1,…,Np
9     for j=1,…,d
10
        u(g)i,j = { v(g)i,j, if randi,j()≤Cr
                  { x(g)i,j, otherwise
#step 4 selection
11  for i=1,…,N
12
        x(g+1)i = { u(g)i, if f(u(g)i)≤f(x(g)i)
                  { x(g)i, otherwise
```

Fig. 2. The canonical DE algorithm.

range $[1, Np]$. These indices are randomly generated for each new vector $v_i^{(g)}$. The scaling factor F is a positive control parameter for scaling the difference vectors.

Through crossover, the vector $v_i^{(g)}$ mixes its components with the target vector $x_i^{(g)}$ to form the trial vector $u_i^{(g)} = \{u_{i,1}^{(g)}, u_{i,2}^{(g)}, \ldots, u_{i,d}^{(g)}\}$. The DE family of algorithms commonly uses two crossover methods: exponential (or two-point modulo) and binomial (or uniform) [19]. In Fig. 2 we described the binomial crossover method, which is performed on each of the d variables whenever a randomly generated number between 0 and 1 is less than or equal to a prefixed parameter Cr called the crossover rate.

The selection determines whether the target vector $x_i^{(g)}$ or the trial vector $u_i^{(g)}$ survives to the next generation, i.e. at $g = g + 1$. The objective function (10) is minimized at this step. Therefore, if the new trial vector yields an equal or lower value of the objective function, it replaces the corresponding target vector in the next iteration; otherwise, the target is retained in the next generation population.

The freely available DE code (de.c file; version 3.6; `www1.icsi.berkeley.edu/~storn/code.html`) was adopted for the purposes of dye molecule optical response simulations. To improve the performance of the program, the DE main cycle was parallelized by using the MPI library. By parallelizing the application, we implemented the obvious way to speed up computations. Among the available nodes for a task, one node is chosen to be the master node to run the main DE routine as well as the simulation procedures. The other nodes are slaves and used to run only the simulation procedures. The population size Np should be chosen according to the following equation: $Np = N_{nodes}k$, $k \in N$, where N_{nodes} is the number of nodes available for computation. The master node controls elementary procedures of the program: loading the experimental data and input parameters and saving the output results. After the initialization of DE is completed and the set of $x_i^{(g)}$ vectors is created, the master node distributes these vectors to all other nodes. Then the calculation of absorption spectrum starts on the slave nodes and including the master node. When the simulation is finished, each node returns the objective function, and then the DE algorithm checks the results for the current best solution and creates a new population according to the selected strategy.

4. RESULTS AND DISCUSSION

Modeling of the optical properties of carotenoids is a very good task for any optimization routine. It requires sequential numerical evaluation of equations (7), (8), and (9). The first step is calculation of the spectral density $C''(\omega)$. In the case of carotenoids, it carries information only about five vibronic modes. This means that $\{\omega_j, S_j, \gamma_j\}$ consists of 15 parameters to be fitted. The lowest mode of the set is very important for simulation of absorption, and $\{\omega_{low}, S_{low}, \gamma_{low}\}$ are free parameters to fit and reflect the influence of the local surrounding on the electronic transition of the dye molecule. However, for the other four modes, ω_j and γ_j can be estimated by applying different optical spectroscopy techniques, namely Raman spectroscopy. The Raman spectra of spheroidene and spheroidenone have four distinct bands at 800–1600 cm^{-1} [9].

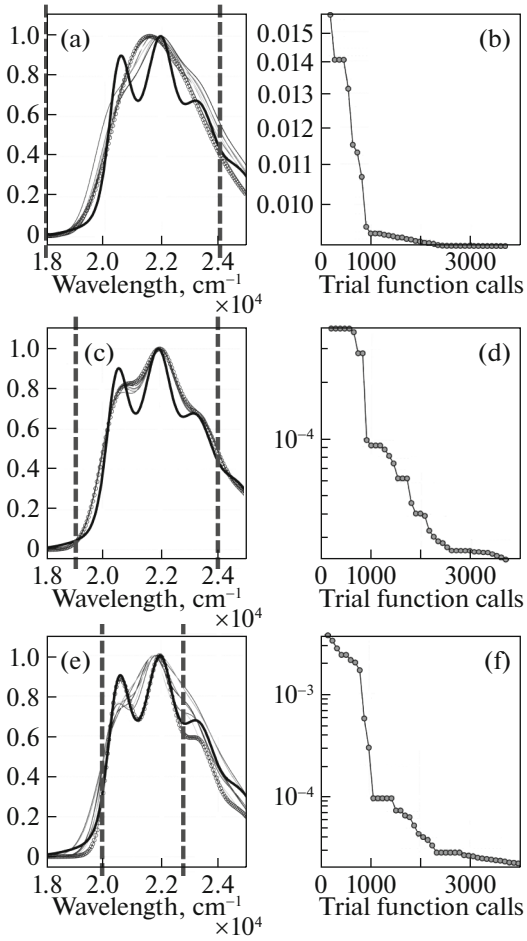

Fig. 3. The effect of the spectral range width on the experimental data fitting. Absorption spectra (a, c, e) of spheroidene in solution fitted by DE and the dependences of $f(x_i^g)$ objective functions on the number of trial function calls (b, d, f) are shown. The thick lines are the experimental data; thin lines are calculated spectra after the first ten degenerations; thin lines with circle markers are the best solutions. Parameters of DE: $DE/best/1/bin$, $F = 0.6$, $Cr = 0.95$, number of generations $Gen_{max} = 40$, number of free parameters $d = 9$, and population size $Np = 90$. Vertical dashed lines mark the boundaries of the spectral region to be fitted. K in equation (10) is the number of points within these boundaries.

Table 1 contains ω_j of high frequency modes obtained from experiment. Similarly, the damping factors are the same for these modes and $\gamma_j = 12$ cm^{-1}. Thus, the number of vibronic mode parameters to search is reduced from 15 to 7.

Integration of equations (8) and (9) requires appropriate resolution for the time and frequency scales: $2^{12} = 4096$ points were used to create the time and frequency arrays. The corresponding time and frequency steps are 0.0024 ps and 3.4180 cm^{-1}. The value of $g(t)$ is temperature dependent, and since spectra were measured at room temperature, $T = 300$ K is set in (8). Equation (9) contains two more

Table 1. Frequencies (ω_i) and intensities (I_i^{norm}) for four vibronic modes (v_i) of the normalized Raman spectra of carotenoids

	v_1		v_2		v_3		v_4	
	ω_1	I_1^{norm}	ω_2	I_2^{norm}	ω_3	I_3^{norm}	ω_4	I_4^{norm}
Spheroidene	1525	0.65	1156	1.0	1004	0.32	968	0.092
Spheroidenone	1520	0.83	1157	1.0	1005	0.30	970	0.086

Table 2. Parameters of the best multimode Brownian oscillator models obtained for the spheroidene and spheroidenone absorption spectra (lines 1, 2) and the results averaged over 10 DE runs (lines 3, 4). Mean values and the standard deviations are given in parenthesis

		Ω_{eg}	$FWHM_{\Omega}$	ω_{low}	S_{low}	γ_{low}	S_{v_1}	S_{v_2}	S_{v_3}	S_{v_4}
1	Spheroidene (Fig. 4a)	22277.0	544.0	499.0	0.8	284.0	0.73	3×10^{-4}	0.39	0.7
2	Spheroidenone (Fig. 4b)	21332.0	1812.0	28.0	0.5	495.0	1.09	0.17	0.01	0.26
3	Spheroidene (averaged)	22269.0 (9.0)	569.0 (274)	395.0 (155)	1.1 (0.6)	148.0 (150)	0.72 (0.01)	0.12 (0.14)	0.31 (0.14)	0.31 (0.28)
4	Spheroidenone (averaged)	21317.0 (69.0)	2031.0 (272.0)	87.0 (167.0)	1.7 (1.0)	292.0 (218.0)	0.96 (0.39)	0.32 (0.3)	0.10 (0.19)	0.32 (0.35)

parameters to fit: the energy of the $|S_0\rangle \rightarrow |S_2\rangle$ electronic transition of carotenoids Ω_{eg} and the FWHM of inhomogeneous broadening $FWHM_{\Omega}$. So, the total number of parameters to fit is 9.

Considering our previous studies on DE [11,25,29], the following set-up was used to run the optimization routine: $DE/best/1/bin$ strategy, $F = 0.6$, $Cr = 0.95$, number of generations $Gen_{max} = 40$, the number of free parameters $d = 9$, and population size $Np = 90$. Ideally, a fitting is successful when the target spectrum and the trial spectrum coincide exactly, i.e. $f(x_i^g) = \chi^2 = 0$ for all frequencies. However, the measured spectra are always slightly different from each other (moreover, the convolution with the hardware function of a device is always present), and what is more important, any quantum model cannot give the exact description of a real system, particularly for a system of electronic and vibronic states of carotenoids. Numerous runs of the DE fitting procedure showed that after 50 generations χ^2 is practically constant and becomes only 15-20 times smaller in comparison with the first generation. However, varying the boundaries of the frequency range ω_k, which is used in the objective function (10), we found that the final ω^2 saturation value can be reduced and the quality of the carotenoid absorption band fine structure fitting can be substantially improved.

The plots in Fig. 3 demonstrate the effect of choosing the frequency range of the experimental spectra $I(\omega_k)$ that is used to determine parameters of the multimode Brownian oscillator model. The full ω_k range of the experimental data is from 15015 to 27026 cm^{-1} with $K = 297$. However, if we run DE calculating the objective function with the full range of frequencies, the convergence of the method will be very poor (Figs. 3a and 3b). The reason forthis phenomenon is that the applied theory is not good enough for modeling the carotenoid optical response at certain frequencies, particularly at 23000 cm^{-1} and higher [24]. Thus, the key to successful processing of the optimizer is the proper choice

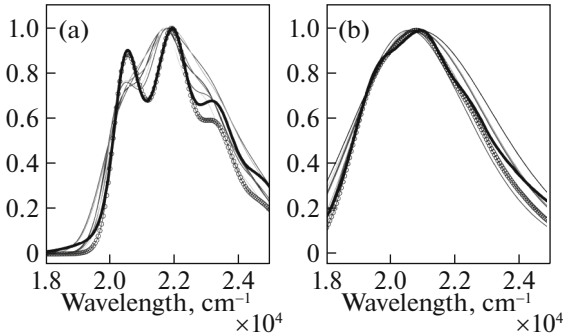

Fig. 4. The best results of spheroidene (a) and spheroidenone (b) absorption fitting obtained after 40 generations (thin lines with circle markers). The thick lines are the experimental data; the thin lines correspond to the best solutions of the first seven generations. The parameters of DE are the same as in Fig. 3.

of an optical range of the studied data. In the case of spheroidene, if we focus our attention at the 20000 cm^{-1}– 22500 cm^{-1} range (Figs. 3e, 3f), DE finds reliable solutions. In the case of spheroidenone, the appropriate range turned out to be 19000 cm^{-1}–23000 cm^{-1}.

The best solutions for the above DE settings are shown in Fig. 4. Parameters of the multimode Brownian oscillator model for the solution is presented in Fig. 4, and the results averaged over 10 runs of the optimizer for spheroidene and spheroidenone are listed in Table 2.

5. CONCLUSIONS

Thus, we have shown that DE allows simulation of absorption spectra of carotenoids in solution. The overall shape and position of all major peaks and minor shoulders of the $|S_0\rangle \rightarrow |S_2\rangle$ electronic transition was predicted with good precision. We got the best coincidence of experimental and calculated absorption for spheroidene and spheroidenone using the $DE/best/1/bin$ strategy and $F = 0.6$, $Cr = 0.95$. To speed up the calculations, the DE code was parallelized using the MPI library. The method of parallelization of the program was as follows: one master node and $(N_{nodes} - 1)$ slave nodes. The DE code runs on the master node, which also controls the data distribution between the slave nodes and collects the intermediate results.

We have shown that the frequency range ω_k of experimental spectra $I(\omega_k)$ that is used to determine the parameters is extremely important. One must choose a frequency range in which the theory describes the experimental data as adequately as possible. Comparing the standard deviation values of fitting parameters, we conclude that the electronic transition energy Ω_{eg}, the full width at half maximum of inhomogeneous broadening $FWHM_\Omega$, S_{v_1}, and S_{v_2} Huang-Rhys factors of the v_1 and v_2 vibronic modes were determined with good precision. The variations of the low frequency mode parameters $\{\omega_{low}, S_{low}, \gamma_{low}\}$ are high enough to consider them reliably defined.

FUNDING

R.Y. Pishchalnikov was supported by the Russian Foundation of Basic Research (RFBR grant no. 19-01-00696). This study was carried out using equipment of the shared research facilities of the HPC computing resources at Moscow State University.

REFERENCES

1. H. Hashimoto, C. Uragami, and R. J. Cogdell, "Carotenoids and photosynthesis," in *Carotenoids in Nature: Biosynthesis, Regulation and Function,* Ed. by C. Stange (Springer, New York, 2016), Vol. 79, pp. 111–139.
2. D. Shevela, R. Y. Pishchainikov, L. A. Eichacker, and Govindjee, "Oxygenic photosynthesis in cyanobacteria," in *Stress Biology of Cyanobacteria: Molecular Mechanism to Cellular Responces* (CRC, Boca Raton, FL, 2013), pp. 3–40. doi 10.1201/b13853-3
3. N. N. Sluchanko, Y. B. Slonimskiy, and E. G. Maksimov, "Features of protein-protein interactions in the cyanobacterial photoprotection mechanism," Biochem. (Moscow) **82**, 1592–1614 (2017). https://doi.org/10.1134/s000629791713003x
4. E. G. Maksimov, N. N. Sluchanko, Y. B. Slonimskiy, E. A. Slutskaya, A. V. Stepanov, A. M. Argentova-Stevens, E. A. Shirshin, G. V. Tsoraev, K. E. Klementiev, O. V. Slatinskaya, E. P. Lukashev, T. Friedrich, V. Z. Paschenko, and A. B. Rubin, "The photocycle of orange carotenoid protein conceals distinct intermediates and asynchronous changes in the carotenoid and protein components," Sci. Rep. **7**, 15548 (2017). https://doi.org/10.1038/s41598-017-15520-4
5. H. Hashimoto, C. Uragami, N. Yukihira, A. T. Gardiner, and R. J. Cogdell, "Understanding/unravelling carotenoid excited singlet states," J. R. Soc. Interface **15**, 20180026 (2018). https://doi.org/10.1098/rsif.2018.0026
6. A. Ashikhmin, Z. Makhneva, M. Bolshakov, and A. Moskalenko, "Incorporation of spheroidene and spheroidenone into light-harvesting complexes from purple sulfur bacteria," J. Photochem. Photobiol. B **170**, 99–107 (2017). https://doi.org/10.1016/j.jphotobiol.2017.03.020
7. S. Mukamel, *Principles of Nonlinear Optical Spectroscopy* (Oxford Univ. Press, New York, Oxford, 1995).
8. T. Polivka and V. Sundstrom, "Dark excited states of carotenoids: Consensus and controversy," Chem. Phys. Lett. **477**, 1–11 (2009). https://doi.org/10.1016/j.cplett.2009.06.011

9. R. Y. Pishchalnikov, I. A. Yaroshevich, T. A. Slastnikova, A. A. Ashikhmin, A. V. Stepanov, E. A. Slutskaya, T. Friedrich, N. N. Sluchanko, and E. G. Maksimov, "Structural peculiarities of keto-carotenoids in water-soluble proteins revealed by simulation of linear absorption," Phys. Chem. Chem. Phys. **21**, 25707–25719 (2019). https://doi.org/10.1039/c9cp04508b
10. R. Pishchalnikov, V. Shubin, and A. Razjivin, "Single molecule fluorescence spectroscopy of PSI trimers from Arthrospira platensis: A computational approach," Molecules **24**, 822 (2019). https://doi.org/10.3390/molecules24040822
11. R. Pishchalnikov, "Application of the differential evolution for simulation of the linear optical response of photosynthetic pigments," J. Comput. Phys. **372**, 603–615 (2018). https://doi.org/10.1016/j.jcp.2018.06.040
12. M. J. Kochenderfer and T. A. Wheeler, *Algorithms for Optimization* (The MIT Press, Cambridge, MA, 2019).
13. M. Mutingi and C. Mbohwa, *Grouping Genetic Algorithms: Advances and Applications* (Springer International, Switzerland, 2017).
14. T. Back, *Evolutionary Algorithms in Theory and Practice: Evolution Strategies, Evolutionary Programming, Genetic Algorithms,* 1st ed. (Oxford Univ. Press, New York, 1996).
15. I. C. Trelea, "The particle swarm optimization algorithm: convergence analysis and parameter selection," Inform. Process. Lett. **85**, 317–325 (2003). https://doi.org/10.1016/s0020-0190(02)00447-7
16. R. Storn, "System design by constraint adaptation and differential evolution," IEEE Trans. Evolut. Comput. **3**, 22–34 (1999). https://doi.org/10.1109/4235.752918
17. R. Storn and K. Price, "Differential evolution—A simple and efficient heuristic for global optimization over continuous spaces," J. Global Optimiz. **11**, 341–359 (1997). https://doi.org/10.1023/A:1008202821328
18. S. Das, S. S. Mullick, and P. N. Suganthan, "Recent advances in differential evolution—An updated survey," Swarm Evolut. Comput. **27**, 1–30 (2016). https://doi.org/10.1016/j.swevo.2016.01.004
19. S. Das and P. N. Suganthan, "Differential evolution: A survey of the state-of-the-art," IEEE Trans. Evolut. Comput. **15**, 4–31 (2011). https://doi.org/10.1109/tevc.2010.2059031
20. W. Siebrand and M. Z. Zgierski, "Franck-Condon effects in resonance Raman-spectra and excitation profiles," J. Chem. Phys. **71**, 3561–3569 (1979). https://doi.org/10.1063/1.438812
21. M. Kuki, H. Nagae, R. J. Cogdell, K. Shimada, and Y. Koyama, "Solvent effect on spheroidene in nonpolar and polar solutions and the environment of spheroidene in the light-harvesting complexes of Rhodobacter-sphaeroides 2.4.1 as revealed by the energy of the (1)a(g)(-)- b-1(u)+ absorption and the frequencies of the vibronically coupled c=c stretching Raman lines in the (1)a(g)(-) and 2(1)a(g)(-) states," Photochem. Photobiol. **59**, 116–124 (1994). https://doi.org/10.1111/j.1751-1097.1994.tb05009.x
22. J. Sue and S. Mukamel, "Solvation dynamics in coherent and spontaneous Raman-spectroscopy—application to beta-carotene," J. Opt. Soc. Am. B **5**, 1462–1472 (1988). https://doi.org/10.1364/josab.5.001462
23. J. A. Burt, X. H. Zhao, and J. L. McHale, "Inertial solvent dynamics and the analysis of spectral line shapes: Temperature-dependent absorption spectrum of beta-carotene in nonpolar solvent," J. Chem. Phys. **120**, 4344–4354 (2004). https://doi.org/10.1063/1.1644534
24. C. Uragami, K. Saito, M. Yoshizawa, P. Molnar, and H. Hashimoto, "Unified analysis of optical absorption spectra of carotenoids based on a stochastic model," Arch. Biochem. Biophys. **650**, 49–58 (2018). https://doi.org/10.1016/j.abb.2018.04.021
25. R. Pishchalnikov, I. Yaroshevich, E. Maksimov, N. Sluchanko, A. Stepanov, D. Buhrke, and T. Friedrich, "Orange carotenoid protein absorption spectra simulation using the differential evolution algorithm," in *Supercomputing. RuSCDays 2019,* Commun. Comput. Inform. Sci. **1129**, 302–312 (2019). https://doi.org/10.1007/978-3-030-36592-9_25
26. R. Kubo, "Generalized cumulant expansion method," J. Phys. Soc. Jpn. **17**, 1100–1120 (1962). https://doi.org/10.1143/JPSJ.17.1100
27. M. Lax, "The Franck-Condon principle and its application to crystals," J. Chem. Phys. **20**, 1752–1760 (1952). https://doi.org/10.1063/1.1700283
28. Y. Tanimura and S. Mukamel, "Real-time path-integral approach to quantum coherence and dephasing in nonadiabatic transitions and nonlinear optical-response," Phys. Rev. E **47**, 118–136 (1993). https://doi.org/10.1103/PhysRevE.47.118
29. R. Pishchalnikov, M. Mueller, and A. Holzwarth, "Theoretical modelling of the optical properties and the exciton dynamics of the isolated PSII reaction centre," Photosynth. Res. **91**, 141 (2007).